*BioImpacts*, **2012**, 2(4), 195-205
doi: 10.5681/bi.2012.023
http://bi.tbzmed.ac.ir/

# Numerical Investigation of Pulsatile Blood Flow in a Bifurcation Model with a Non-Planar Branch: The Effect of Different Bifurcation Angles and Non-Planar Branch

**Omid Arjmandi-Tash[1], Seyed Esmail Razavi[2*]**

[1]*Process Design and Simulation Research Center, School of Chemical Engineering, University of Tehran, Tehran, Iran*
[2]*School of Mechanical Engineering, University of Tabriz, Tabriz, Iran*

**ARTICLE INFO**

***Article Type:***
Research Article

***Article History:***
Received: 03 June 2012
Revised: 07 July 2012
Accepted: 11 July 2012
ePublished: 31 July 2012

***Keywords:***
Atherosclerosis
Arterial bifurcations
Bifurcation Angle
Non-Planar Branch
Pulsatile Flow
Wall Shear Stress

**ABSTRACT**

***Introduction:*** Atherosclerosis is a focal disease that susceptibly forms near bifurcations, anastomotic joints, side branches, and curved vessels along the arterial tree. In this study, pulsatile blood flow in a bifurcation model with a non-planar branch is investigated. ***Methods:*** Wall shear stress (WSS) distributions along generating lines on vessels for different bifurcation angles are calculated during the pulse cycle. ***Results:*** The WSS at the outer side of the bifurcation plane vanishes especially for higher bifurcation angles but by increasing the bifurcation angle low WSS region squeezes. At the systolic phase there is a high possibility of formation of a separation region at the outer side of bifurcation plane for all the cases. WSS peaks exist on the inner side of bifurcation plane near the entry section of daughter vessels and these peaks drop as bifurcation angle is increased. ***Conclusion:*** It was found that non-planarity of the daughter vessel lowers the minimum WSS at the outer side of the bifurcation and increases the maximum WSS at the inner side. So it seems that the formation of atherosclerotic plaques at bifurcation region in direction of non-planar daughter vessel is more risky.

## Introduction

Atherosclerosis is a disease of the arteries characterized by the deposition of plaques of fatty material on vessel walls (Malek *et al* 1999, Nixon *et al* 2010). Low shear stress, high vessel pressure distribution and high particle residence time in the region of the atherosclerosis are considered as three risk factors for the development of such intimal thickenings (Chytilová and Malík 2007, Cecchi *et al* 2011).

Since arterial bifurcations are one of the most important susceptible locations for formation of atherosclerotic plaques, a lot of researches have been done so far targeting the analysis and prediction of this phenomena in bifurcations experimentally (Friedman *et al* 1993, Schulz and Rothwell 2001, Zhang *et al* 2010), theoretically (Perktold *et al* 1991a, Lu *et al* 2002, Chen and Lu 2004, 2006, Tadjfar 2006, Bressloff 2007, Nguyen *et al* 2008, Fan *et al* 2009, Arjmandi-Tash *et al* 2011) or in a combined manner (Perktold *et al* 1991b, Wells *et al* 1996, Marshall *et al* 2004, Lee *et al* 2008). They investigated local hemodynamics governed by the rheological properties of blood and geometrical factors of bifurcations such as proximal area ratio, distal area ratio, bifurcation tortuosity, bifurcation angle and planarity. Chen and Lu (2004, 2006) constructed a hypothetical three-dimensional non-planar artery with bifurcation and numerically investigated the steady and pulsatile flow of non-Newtonian fluid in this bifurcation model. They found that the non-planarity of blood vessels is important factor in hemodynamics and plays a significant role in vascular biology and pathophysiology. On the other hand, Perktold *et al* (1991a) and Fan *et al* (2009) numerically compared non-Newtonian and Newtonian models in the human carotid artery bifurcation. They concluded that blood can be considered as a Newtonian fluid with good approximation. By doing some in vitro experiments, Friedman *et al* (1993) investigated the relationship between the angle formed by the left circumflex and left anterior descending coronary arteries at the bifurcation of the left main coronary artery. Their results showed a small branching angle may be a geometric risk factor for proximal atherosclerotic disease in daughter vessels. From the other point of view, Perktold *et al*

***Corresponding authors:** Seyed Esmail Razavi (PhD), Email: razavi {at} tabrizu.ac.ir

(1991b) and Wells *et al* (1996) analyzed flow and stress patterns in human carotid artery bifurcation models with different bifurcation angles. Their findings did not confirm the Friedman *et al* (1993) results and indicated that the hemodynamic phenomena are more pronounced in the large angle carotid bifurcation. Similarly, Nguyen *et al* (2008) concluded that larger bifurcation angles and larger off-plan angles lower the WSS on the sinus wall, hence increasing the risk of plaque build-up. Also, Lee *et al* (2008) investigated geometric risk factors on deposition of plaques and demonstrated that there is not any significant relationship between disturbed flow and both bifurcation angle and planarity.

Reviewing the literature shows that there are various conclusions about the influence of bifurcation angle on development of atherosclerotic plaques; thus it motivates us to carry out the present study. A comprehensive analysis of the influence of different bifurcation angles on WSS distribution and formation of separation regions is presented in this report. This work also lies in the effect of non-planarity of one daughter vessel on the flow pattern in planar bifurcation location for different bifurcation angles. Three pulse cycle time-averaged WSS distributions are illustrated to simplify complex cardiac cycle of values. Such analysis may lead us to predict the risk factors for atherosclerosis in a real condition.

## Materials and methods

In this paper, the hypothetical model of Lu *et al* (Lu *et al* 2002, Chen and Lu 2004, 2006) for an arterial bifurcation with a non-planar daughter branch is utilized. The mother vessel's length before bifurcation is set to 3D where D is the diameter of all the vessels. This vessel is symmetrically divided into two daughter vessels with an angle θ in between. After bifurcation, one of the vessels continues planar for 1.5D length and then undergoes a 45˚ bending with a radius of 4D before it straightens up for a further length of 4D. This is what is referred to by non-planar branch. Another daughter vessel is straight in-plane for a length of 8D. A schematic representation of this bifurcation is shown in Fig. 1. As suggested in (Perktold *et al* 1991b), D = 6.2 mm is used in the calculations. On the other hand and while in the original model, two daughter vessels are normal to each other, cases with 60˚ and 75˚ between the daughter vessels are also considered in the present study to explore the effect of bifurcation angle.

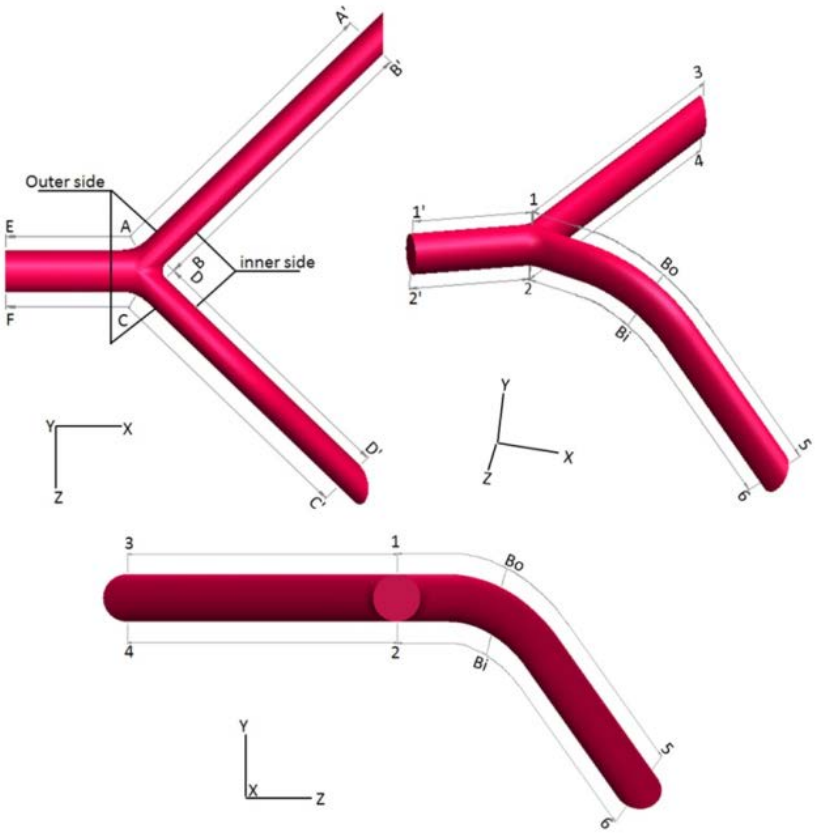


**Fig. 1.** Bifurcation model with planar and non-planar daughter vessels.

Considering blood as incompressible and Newtonian fluid (Perktold *et al* 1991a, Fan *et al* 2009), the Navier–Stokes equations are expressed as followings (Bird *et al* 2002):

(1): $$\nabla \cdot u = 0$$

(2): $$\rho\left(\frac{\partial u}{\partial t} + u \cdot \nabla u\right) = -\nabla p + \mu \nabla^2 u$$

Where, u denotes the velocity vector and *p* the pressure, $\rho$ and $\mu$ refer to the density and dynamic viscosity, respectively. The values of $\rho$ and $\mu$ are set to 1030kg/m3 and 0.004 Pa.s (Nguyen *et al* 2008).

Similar to (Perktold *et al* 1991b), the flow at the inlet of mother vessel is considered pulsatile with a periodicity of T = 0.8334 s (proportional to 72 beat per minute) as shown in Fig. 2.

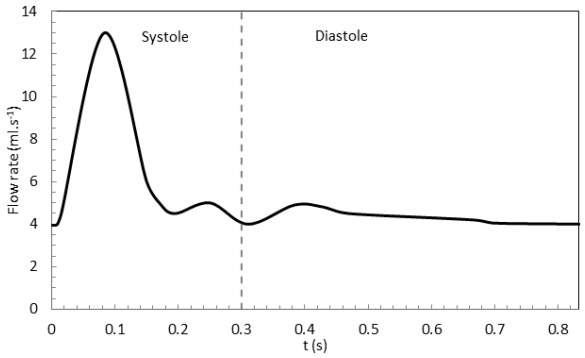


**Fig. 2.** Pulsatile flow rate curve in the common carotid with period T = 0.8334 s.

Inlet Reynolds number varies between 206 (end of diastole) to 687 (peak systole) and the Womersley number based on the period of the flow pulse is equal to 4.32. At inlet of mother vessel, Womersley boundary conditions with time-dependent velocity profiles are imposed. At the vessel wall, the no-slip condition and at the exit of each daughter vessel, constant pressure and zero axial velocity gradient are used. The governing equations can be solved by using a time-accurate finite element method based on fractional-step velocity correction (Lu *et al* 2002, Chen and Lu 2004, 2006, Kovacs and Kawahara 1991). The Galerkin finite element (Kovacs and Kawahara 1991) is applied to non-uniformly grid of 262544, 276520 and 286469 quadratic tetrahedral elements for 90˚, 75˚ and 60˚ bifurcation angles, respectively. The grids are clustered near the walls in radial direction where high variable gradients are expected.

**Results and discussion**

To validate the calculations, we tried to re-solve the problem of a pulsatile flow of Newtonian fluid in 90° bifurcation angle model, similar to what was investigated by Chen and Lu (2006). Fig. 3 compares the results of two calculations and shows they are in good agreement. This verifies our computational code.

Distributions of WSS along generating lines on vessels are shown in Figs. 4-9 at peak systole and the end of diastole. Also Figs. 10-12 illustrate three pulse cycle time-averaged distributions of WSS. In all the cases, horizontal axis indicates the position on generating lines with respect to the exit of mother vessel at the point of bifurcation. Comparisons of WSS at peak systole (Figs. 4-6) and end of diastole (Figs. 7-9) reveal the fact that by increasing mean velocity and thinning the viscous boundary layer at peak systole, WSS increases during systolic phase for three bifurcation angles.

Figures 4, 7 and 10 give the distributions of WSS along four generating lines on the mother vessels for different bifurcation angles at peak systole, end of diastole and pulse cycle time-average, respectively. As shown in Figs. 4(a,b), 7(a,b) and 10(a,b), WSSs decrease at bifurcation region along lines 1'-1 and 2'-2. Decrease is more remarkable for 90˚ bifurcation angle at peak systole (83% decrease) in comparison with the end of diastole (80% decrease). In addition, this WSS drop occurs closer to the apex of bifurcation for the case of 60˚ bifurcation angle compared to the other cases. On the other hand, distributions of WSS along lines E-A and F-C in Figs. 4(c,d), 7(c,d) and 10(c,d) show that just before the bifurcation region, WSSs increase, especially for 90˚ bifurcation angle.

Figs. 5, 8 and 11 also give the distributions of WSS along the generating lines on the planar daughter vessel for three bifurcation angles at peak systole, end of diastole and pulse cycle time-average, respectively. As shown in Figs. 5(a,b), 8(a,b) and 11(a,b), WSSs increase along lines 1-3 and 2-4 near the inlet of planar daughter vessel and then decrease and become stable. This behavior is more remarkable at peak systole and for the case of 90˚ bifurcation angle. Also these figures show that, the WSS peaks come closer to the entry section of daughter vessel as bifurcation angle increases. On the other hand, at the outer side of the bifurcation plane along lines A-A' in Figs. 5(c), 8(c) and 11(c), WSSs decrease considerably. With Increasing the bifurcation angle, the position of minimum WSS along line A-A' approaches the entry section of the daughter vessel. After these drops, WSSs increase specially for larger bifurcation angles and become almost stable soon. Results of the minimum WSSs along line A-A' for different bifurcation angles are summarized in Table 1. It is clear in this table that the case with 90˚ bifurcation angle has the least WSS at the peak systole amongst the

others. Just the other way around, Figs. 5(d), 8(d) and 11(d) show that immediately after the stagnation region at apex of bifurcation, WSS suddenly peaks up to a maximum value along line B-B' and then saturates in a low value downstream of the flow.Comparison of the maximum values of WSS along this line (Table 2) illustrates that WSS for the case of 60˚ bifurcation angle and at peak systole is the largest among the others. Nevertheless, this initial peak falls faster for lower bifurcation angles as one moves away from the bifurcation apex, resulting in lower WSS at lower bifurcation angles.

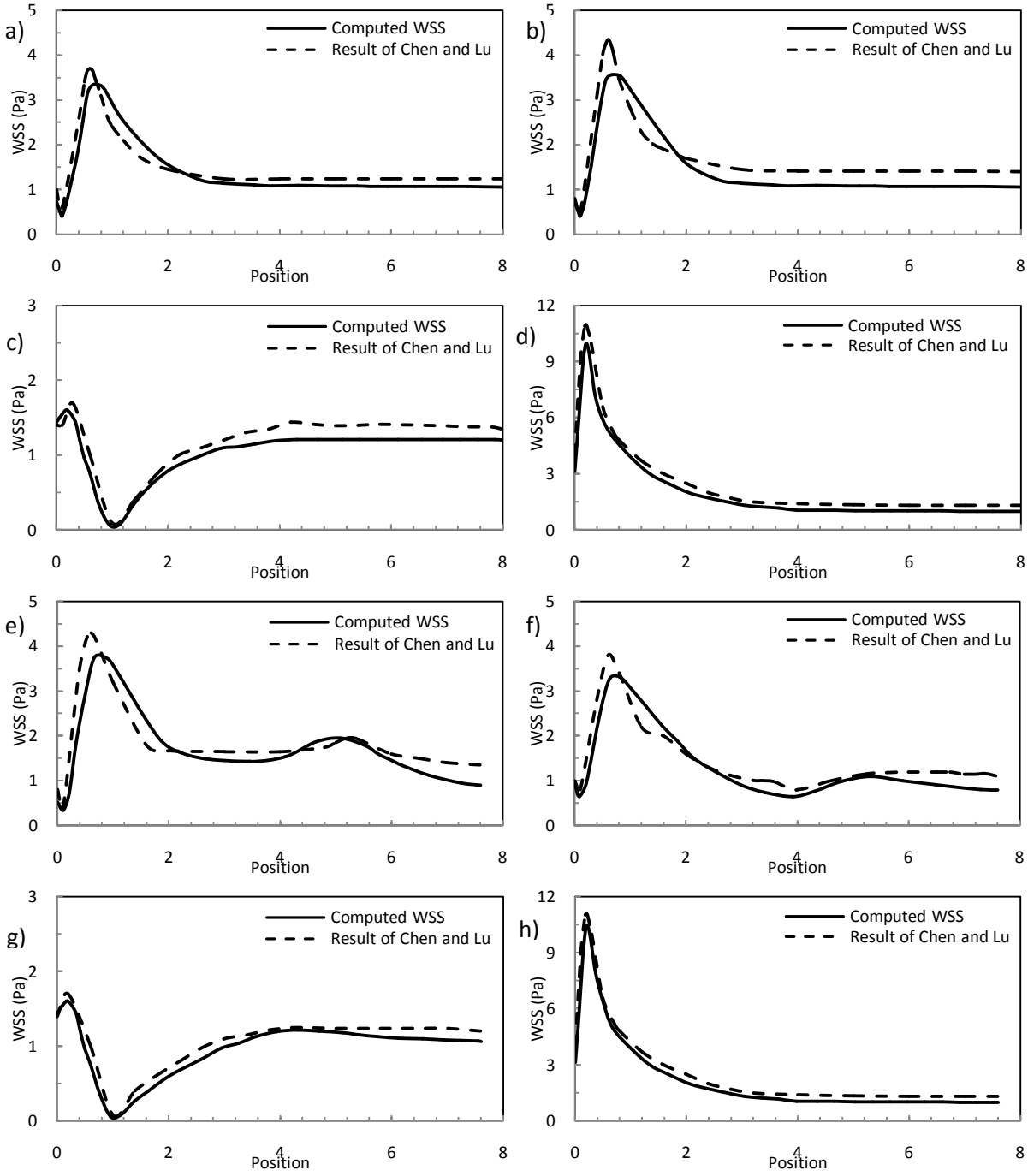


**Fig. 3.** Comparison of the computed WSS distributions for 90° bifurcation angle along generating lines on daughter vessels with the results of Chen and Lu (2006) at peak systole: a) 1-3; b) 2-4; c) A-A'; d) B-B'; e) 1-5; f) 2-6; g) C-C'; h) D-D'.

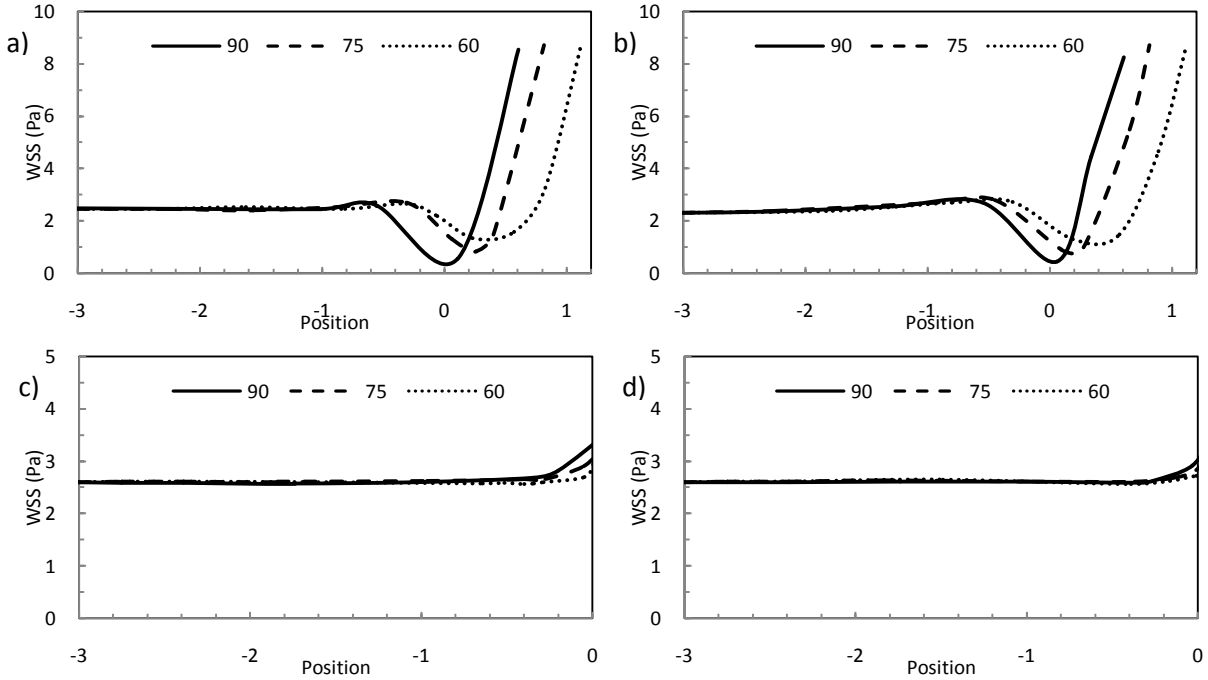


**Fig. 4.** Distributions of WSS along four generating lines on the mother vessels at peak systole for three bifurcation angles: a) 1'-1; b) 2'-2; c) E-A; d) F-C.

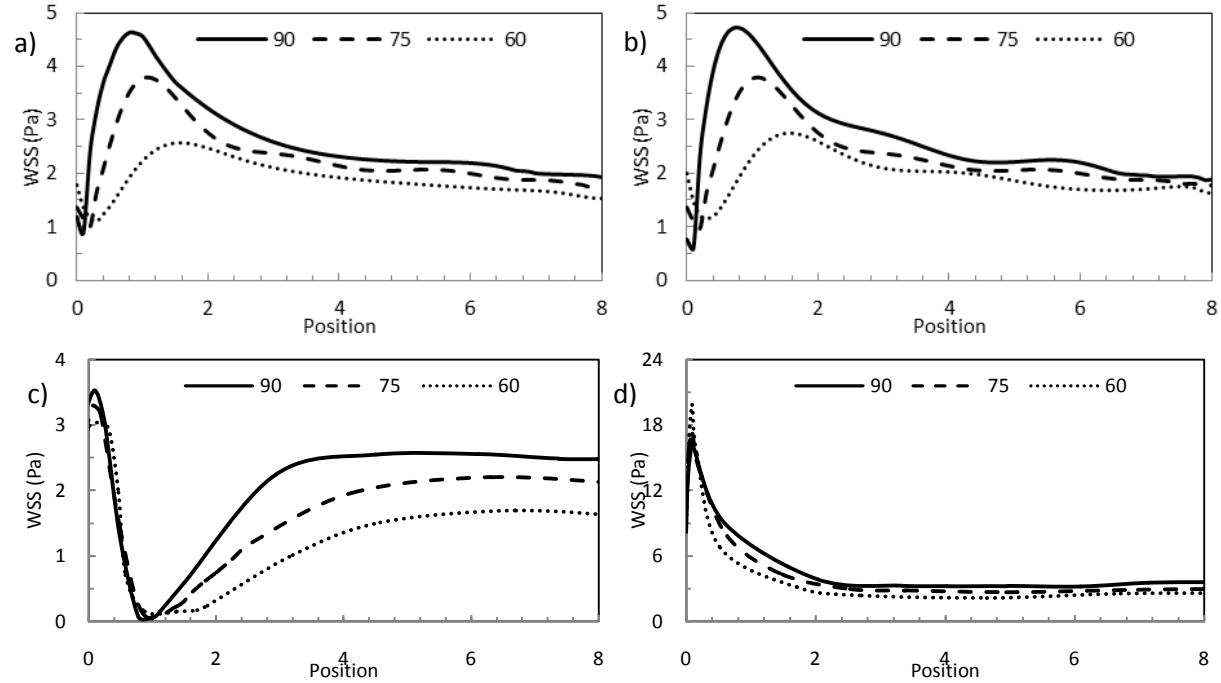


**Fig. 5.** Distributions of WSS along four generating lines on the planar daughter vessels at peak systole for three bifurcation angles: a) 1-3; b) 2-4; c) A-A'; d) B-B'.

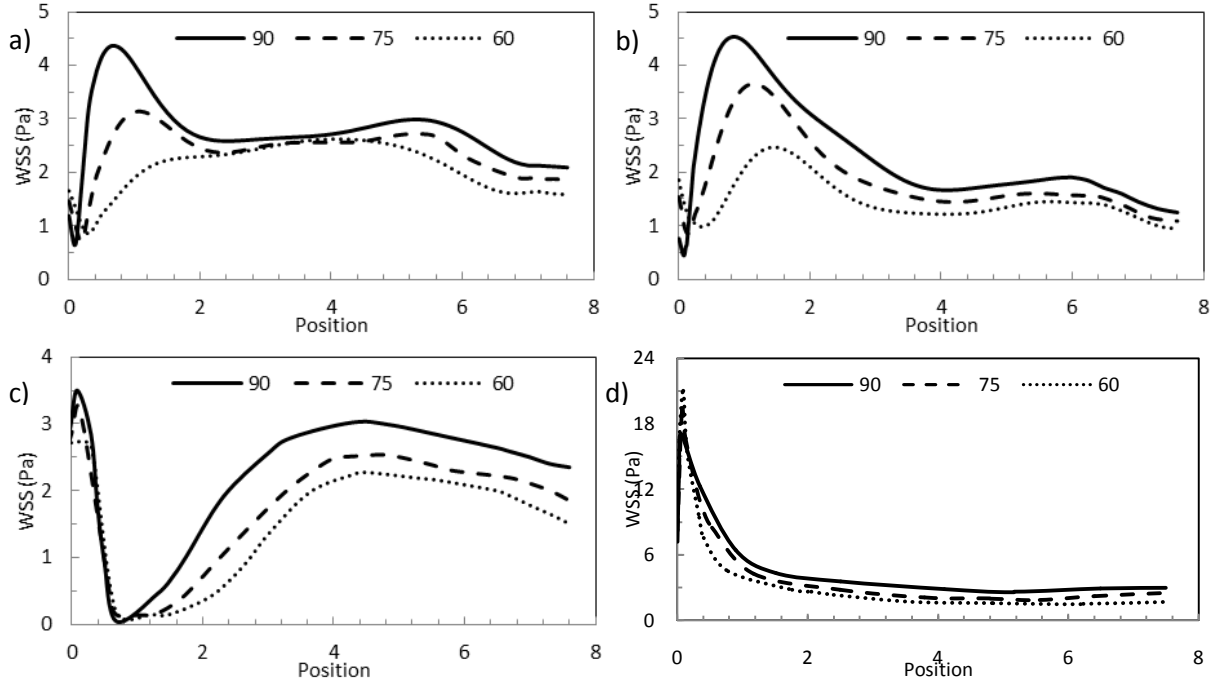


**Fig. 6.** Distributions of WSS along four generating lines on the non-planar daughter vessels at peak systole for three bifurcation angles: a) 1-5; b) 2-6; c) C-C'; d) D-D'.

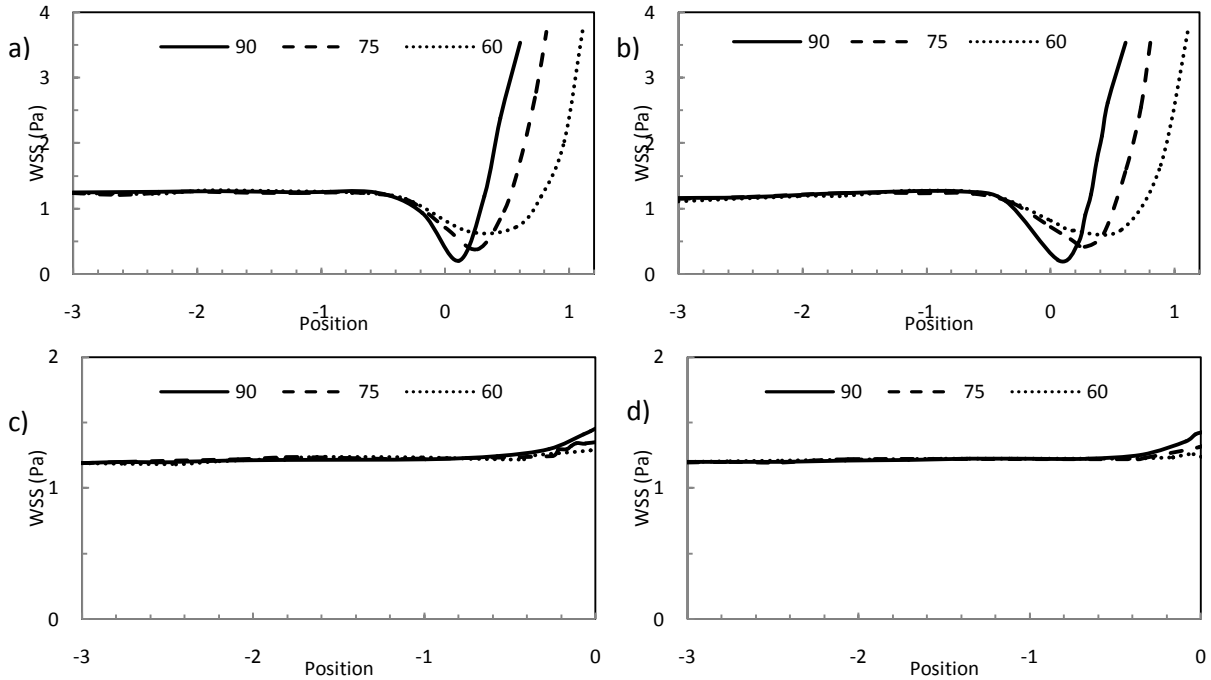


**Fig. 7.** Distributions of WSS along four generating lines on the mother vessels at the end of diastole for three bifurcation angles: a) 1'-1; b) 2'-2; c) E-A; d) F-C.

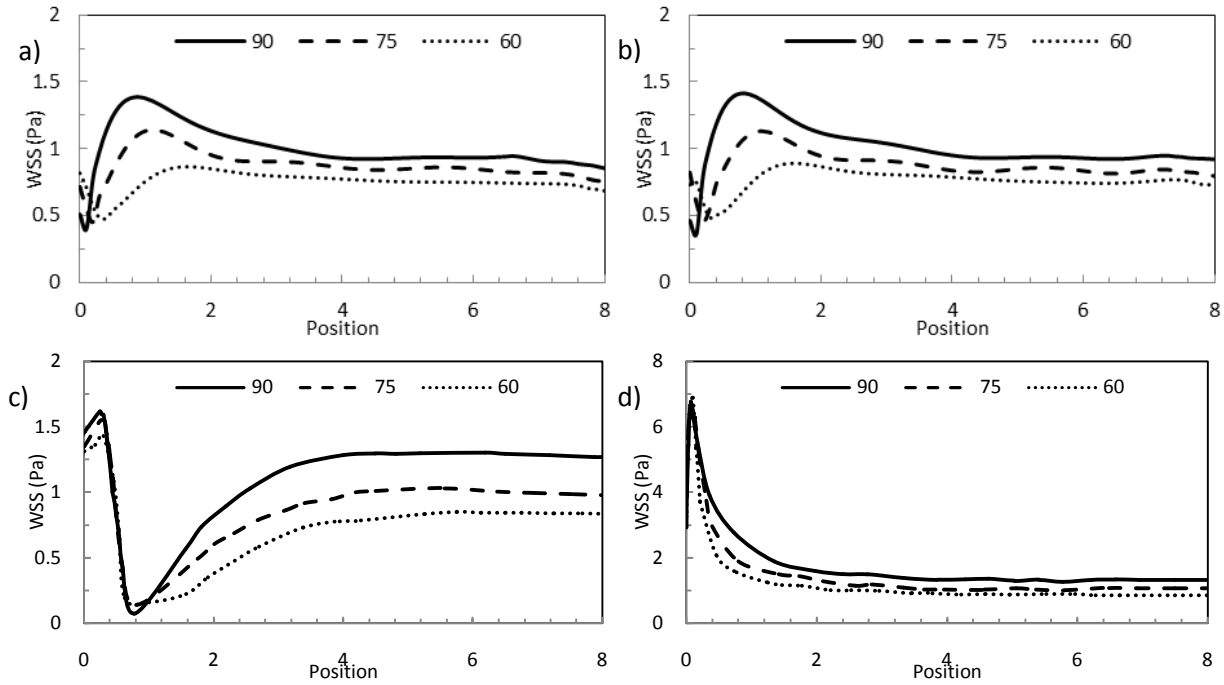


**Fig. 8.** Distributions of WSS along four generating lines on the planar daughter vessels at the end of diastole for three bifurcation angles: a) 1-3; b) 2-4; c) A-A'; d) B-B'.

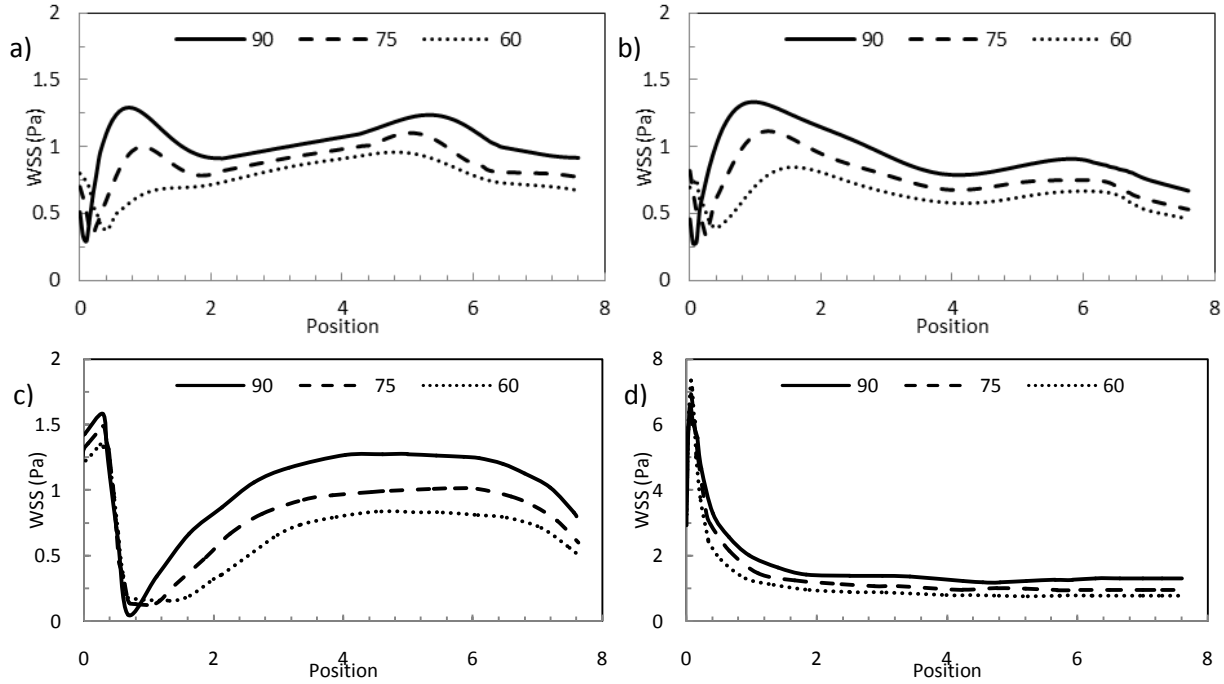


**Fig. 9.** Distributions of WSS along four generating lines on the non-planar daughter vessels at the end of diastole for three bifurcation angles: a) 1-5; b) 2-6; c) C-C'; d) D-D'.

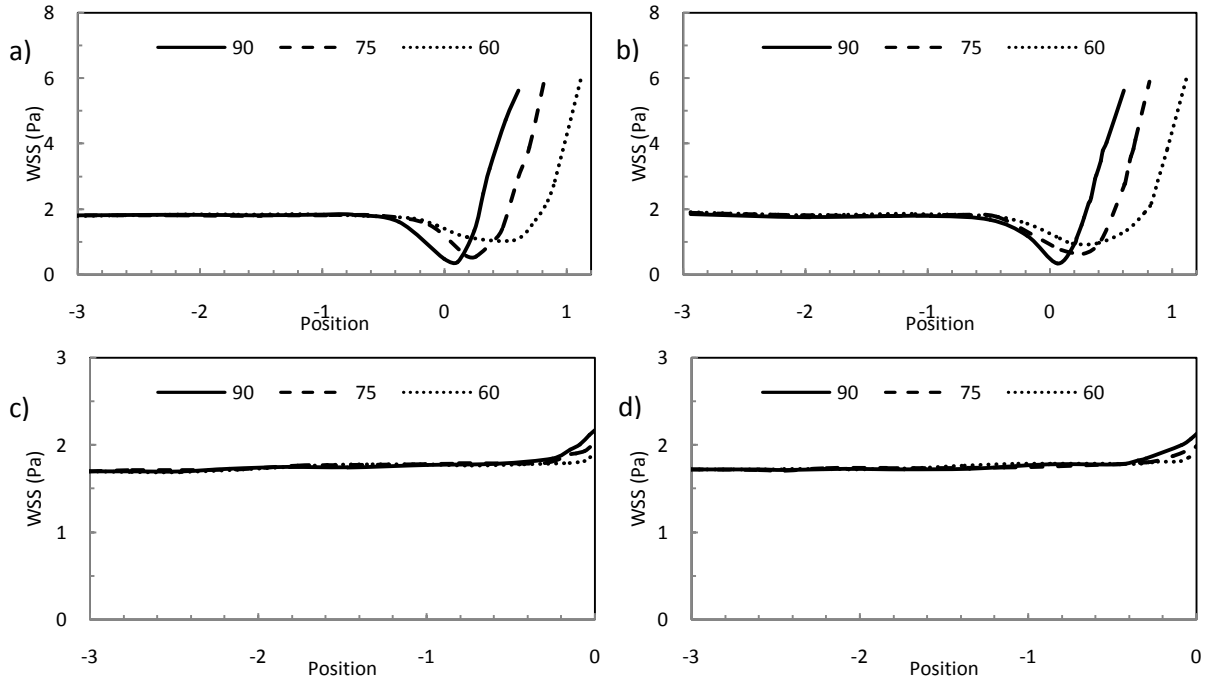


**Fig. 10.** Time-averaged distributions of WSS along four generating lines on the mother vessels for three bifurcation angles: a) 1'-1; b) 2'-2; c) E-A; d) F-C.

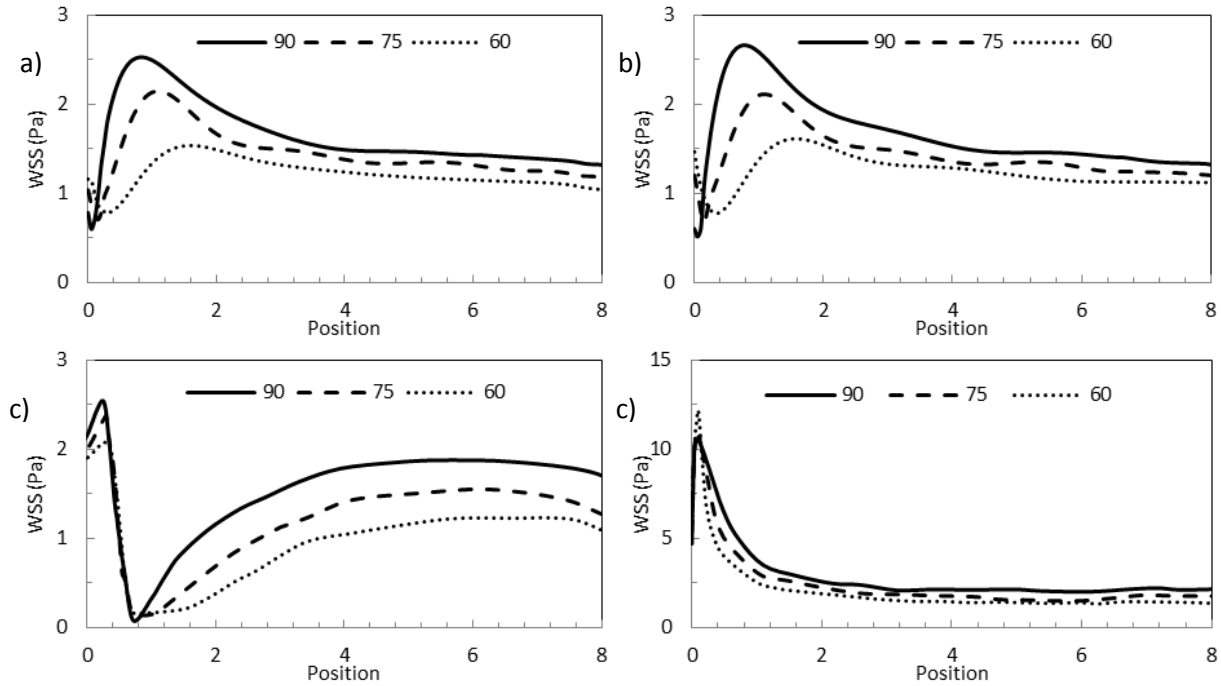


**Fig. 11.** Time-averaged distributions of WSS along four generating lines on the planar daughter vessels for three bifurcation angles: a) 1-3; b) 2-4; c) A-A'; d) B-B'.

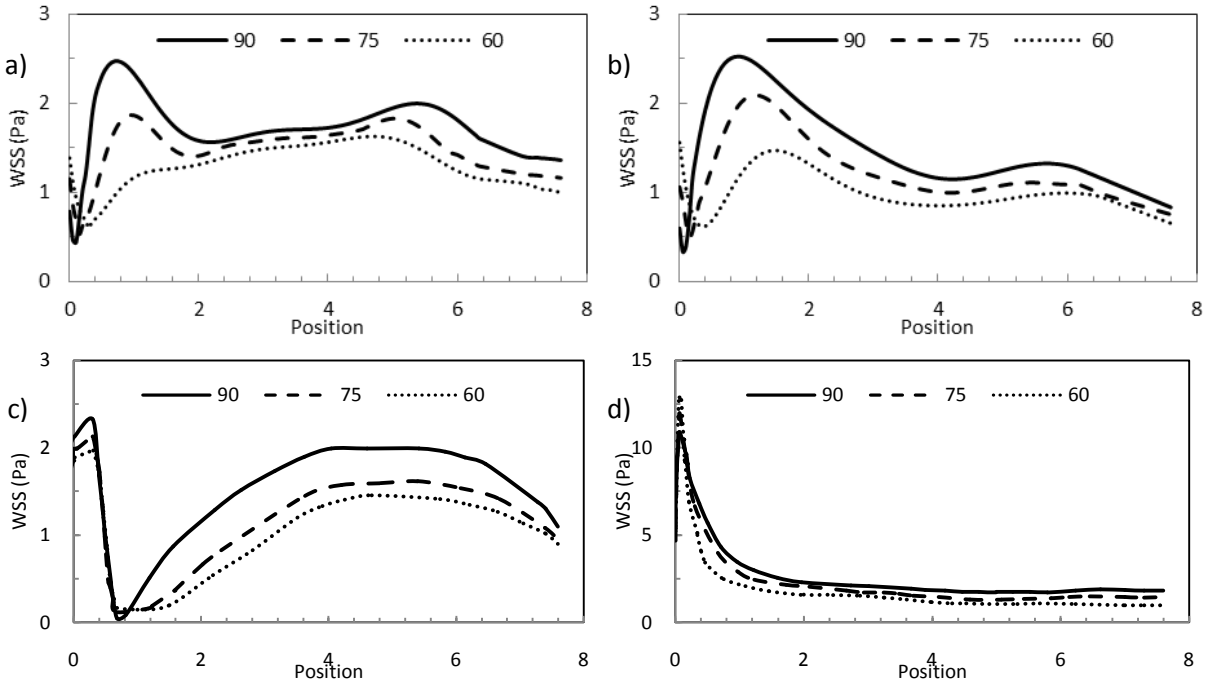


**Fig. 12.** Time-averaged distributions of WSS along four generating lines on the non-planar daughter vessels for three bifurcation angles: a) 1-5; b) 2-6; c) C-C'; d) D-D'.

**Table 1.** Minimum values of WSS along generating lines on vessels for three bifurcation angles, (the unit of values is Pa)

| | Minimum WSS at peak systole | | Minimum WSS at end of diastole | | Minimum time average WSS | |
|---|---|---|---|---|---|---|
| Bifurcation angle | Line A-A' | Line C-C' | Line A-A' | Line C-C' | Line A-A' | Line C-C' |
| 90˚ | 0.0699 | 0.0454 | 0.0751 | 0.0520 | 0.0734 | 0.0502 |
| 75˚ | 0.1278 | 0.1170 | 0.1397 | 0.1305 | 0.1351 | 0.1280 |
| 60˚ | 0.1517 | 0.1431 | 0.1606 | 0.1577 | 0.1583 | 0.1503 |

**Table 2.** Maximum values of WSS along generating lines on vessels for three bifurcation angles, (the unit of values is Pa)

| | Maximum WSS at peak systole | | Maximum WSS at end of diastole | | Maximum time average WSS | |
|---|---|---|---|---|---|---|
| Bifurcation angle | Line B-B' | Line D-D' | Line B-B' | Line D-D' | Line B-B' | Line D-D' |
| 90˚ | 16.3563 | 17.0361 | 6.4992 | 6.5963 | 10.5700 | 10.8951 |
| 75˚ | 17.2207 | 19.1308 | 6.7564 | 6.9376 | 11.0656 | 11.9666 |
| 60˚ | 19.8435 | 21.0329 | 6.8840 | 7.3449 | 12.1570 | 12.8866 |

The distributions of WSS along four generating lines on non-planar daughter vessel for three bifurcation angles at peak systole, end of diastole and pulse cycle time-average are presented in Figs. 6, 9 and 12, respectively. As shown in Figs. 6(a), 9(a) and 12(a), the distributions of WSS along line 1-5 at the entry section of non-planar daughter vessel are similar to the distributions of WSS along lines 1-3, but moving to outer side of the bend, WSS values increase to get local maximums at the vicinity of Bo point. This local maximum for the case of 60˚ bifurcation angle and at the end of diastole is the absolute maximum of WSS along lines 1-5. This shows that the bending has a stronger effect than the bifurcation on increasing the WSS values for the case of 60˚. Also, as shown in Figs. 6(b), 9(b) and 12(b), the distributions of WSS along lines 2-6 at the entry section of non-planar daughter vessel are similar to the distributions of WSS along lines 2-4, but as moving to the inner side of bend, the WSS values decrease to get local minimum at the vicinity of Bi point. WSS profiles along lines C-C' and D-D' in Figs. 6(c,d), 9(c,d) and 12(c,d) are similar to the WSS distributions along lines A-A' and B-B, respectively; however there are slightly difference along lines C-C' and A-A'. Also in contrary with the line A-A', the WSS values along line C-C' decrease gradually after the bending region.

Comparison of the minimum WSSs along lines A-A' and C-C' (Table 1) shows that the minimum values along line C-C' are lower than the values along line A-A'. Also Table 2 shows that the maximum WSSs along line D-D' are higher than the maximum values along line B-B' for all the cases. This reveals the effect of non-planar branch on the WSS distribution at bifurcation region.

## Conclusion

Wall shear stress on the vessel wall is an important risk factor for the development of atherosclerosis since it is believed that the atherosclerotic plaques form in the regions of low WSS. In this study a bifurcation model with a non-planar daughter vessel is analyzed numerically under physiologically relevant pulsatile blood flow. WSS distributions during blood pulses are illustrated for different bifurcation angles.

WSS values are low in two locations in mother vessel, in the vicinity of the points 1 and 2. These locations are prone to separation due to the existence of stagnation regions of dividing surface, more considerable for high bifurcation angles and for high values of the incoming flow Reynolds number (peak systole). Minimum WSS occurs at the outer side of the bifurcation plane, in the vicinity of points A and C, where it approaches to zero. These locations are also prone to separation. At the outer side of bifurcation plane, the minimum values of WSS decline at higher bifurcation angles. These observations are in good agreement with the last reports (Tadjfar 2006, Nguyen *et al* 2008, Perktold *et al* 1991b, Wells *et al* 1996) but not absolutely refuse the conclusion of Friedman *et al* (1993) because, on the other hand, increasing the bifurcation angle squeezes low WSS region. In other words, a decisive conclusion on the issue that which bifurcation angles favor the development of atherosclerotic lesions is strongly dependent on the criterion around WSS value. Higher bifurcation angles are more susceptible locations for the deposition of plaques in the case that lower minimum value of WSS is considered as criterion and if bigger low WSS region is supposed to be criterion, lower bifurcation angles will be more susceptible branches for development of atherosclerotic lesions. Furthermore, at systolic phase there is a higher possibility of formation of a separation region at the outer side of the bifurcation plane for all the angles. Maximum WSSs happen on the inner wall in bifurcation plane and these peaks fall in higher bifurcation angles. This is due to the fact that the flow has not turned far from the wall at the inlet of daughter vessels and there is a large component of normal velocity gradient as well as axial wall gradient in the normal direction.

The non-planarity of daughter vessel lowers the minimum WSS at the outer side of bifurcation plane and increases the maximum WSS at inner side. This is due to the fact that the non-planarity in the daughter vessel swerves the flow from the outer side to the inner side of bifurcation at the side of non-planar branch. So, it seems that the formation of a separation region and atherosclerotic plaques at the outer side of bifurcation plane at the side of non-planar daughter vessel is more risky. Moreover, the non-planarity in the daughter vessel shifts the streamlines of the flow from the inner to the outer side of bend.

All these findings confirm that there are, indeed, several geometrical factors that affect the local hydrodynamic and WSS distributions at bifurcation regions and they can alter the residence time of particles and biological cells in the vicinity of vascular endothelium.

## Ethical issues

None to be declared.

## Competing interests

The authors declare no competing interests.

## References

Arjmandi-Tash O, Razavi SE and Zanbouri R. **2011**. Possibility of Atherosclerosis in an Arterial Bifurcation Model. *BioImpacts*, 1(4), 225-228.

Bird RB, Stewart WE and Lightfoot EN. **2006**. *Transport Phenomen*. 2nd Ed. New York, John Wiley and Sons.

Bressloff NW. **2007**. Parametric geometry exploration of the human carotid artery bifurcation. *J Biomech*, 40(11), 2483-2491.

Cecchi E, Giglioli C, Valente S, Lazzeri C, Gensini GF, Abbate R, *et al*. **2011**. Role of hemodynamic shear stress in cardiovascular disease. *Atherosclerosis*, 214(2), 249-256.

Chen J and Lu XY. **2004**. Numerical investigation of the non-Newtonian blood flow in a bifurcation model with a non-planar branch. *J Biomech*, 37(12), 1899-1911.

Chen J and Lu XY. **2006**. Numerical investigation of the non-Newtonian pulsatile blood flow in a bifurcation model with a non-planar branch. *J Biomech*, 39(5), 818-832.

Chytilová E and Malík J. **2007**. Wall shear stress in carotid artery and its role in the development of atherosclerosis. *Vnitr Lek*, 53(4), 377-381.

Fan Y, Jiang W, Zou Y, Li J, Chen J and Deng X. **2009**. Numerical simulation of pulsatile non-Newtonian flow in the carotid artery bifurcation. *Acta Mech Sin*, 25(2), 249-255.

Friedman MH, Brinkman AM, Qin JJ and Seed WA. **1993**. Relation between coronary artery geometry and the distribution of early sudanophilic lesions. *Atherosclerosis*, 98(2), 193-199.

Kovacs A and Kawahara M. **1991**. A finite element scheme based on the velocity correction method for the solution of the time-dependent incompressible Navier-Stokes equations. *International Journal for Numerical Methods in Fluids*, 13(4), 403-423.

Lee SW, Antiga L, Spence JD and Steinman DA. **2008**. Geometry of the carotid bifurcation predicts its exposure to disturbed flow. *Stroke*, 39(8), 2341-2347.

Lu Y, Lu X, Zhuang L and Wang W. **2002**. Breaking symmetry in non-planar bifurcation: distribution of flow and wall shear stress. *Biorheology*, 39(3-4), 431-436.

Malek AM, Alper SL and Izumo S. **1999**. Hemodynamic shear stress and its role in atherosclerosis. *JAMA*, 282(21), 2035-2042.

Marshall I, Zhao S, Papathanasopoulou P, Hoskins P and Xu Y. **2004**. MRI and CFD studies of pulsatile flow in healthy and stenosed carotid bifurcation models. *J Biomech*, 37(5), 679-687.

Nguyen KT, Clark CD, Chancellor TJ and Papavassiliou DV. **2008**. Carotid geometry effects on blood flow and on risk for vascular disease. *J Biomech*, 41(1), 11-19.

Nixon AM, Gunel M and Sumpio BE, **2010**. The critical role of hemodynamics in the development of cerebral vascular disease. *J Neurosurg*, 112(6), 1240-1253.

Perktold K, Resch M and Florian H. **1991a**. Pulsatile non-Newtonian flow characteristics in a three-dimensional human carotid bifurcation model. *J Biomech Eng*, 113(4), 464-475.

Perktold K, Peter RO, Resch M and Langs G, **1991b**. Pulsatile non-Newtonian blood flow in three-dimensional carotid bifurcation models: a numerical study of flow phenomena under different bifurcation angles.. *J Biomed Eng*, 13(6), 507-515.

Schulz UG and Rothwell PW. **2001**. Major variation in carotid bifurcation anatomy: a possible risk factor for plaque development?. *Stroke*, 32(11), 2522-2529.

Tadjfar M. **2006**. Flow into an Arterial Branch Model. *J Eng Math*, 54(4), 359-374.

Wells DR, Archie JJ and Kleinstreuer C. **1996**. Effect of carotid artery geometry on the magnitude and distribution of wall shear stress gradients.. *J Vasc Surg*, 23(4), 667-78.

Zhang Q, Steinman DA and Friedman MH. **2010**. Use of factor analysis to characterize arterial geometry and predict hemodynamic risk: application to the human carotid bifurcation. *J Biomech Eng*, 132(11), 114505.